

## Transport estimates at the western section of the Strait of Gibraltar: A combined experimental and numerical modeling study

A. Sánchez-Román,<sup>1</sup> G. Sannino,<sup>2</sup> J. García-Lafuente,<sup>1</sup> A. Carillo,<sup>2</sup>  
and F. Criado-Aldeanueva<sup>1</sup>

Received 15 July 2008; revised 10 February 2009; accepted 2 March 2009; published 3 June 2009.

[1] Three-yearlong time series of Acoustic Doppler Current Profiler (ADCP) observations at a single station in Espartel Sill (Strait of Gibraltar) were used to compute an outflow of  $Q_2 = -0.82$  Sv through the main channel. The cross-strait structure of the velocity field or the outflow through a secondary channel north of the submarine ridge of Majuan in Espartel section is not captured by observations so that an improved version of a numerical model (CEPOM) has been used to fill the observational gap. Previously, the model performance has been checked against historical data sets by comparing harmonic constants of the main diurnal and semidiurnal constituents from observed and modeled data at different sites of the strait. Considering the great complexity of tidal dynamics in the area, the comparison is quite satisfactory and validates the model to infer the exchange at longer timescales. Using a “climatological” April in the simulation, extracting a “single station” from the model at the same position as the monitoring station and processing the data similarly, the model gives an outflow through the southern channel 13% higher than observations. The inclusion of the cross-strait structure of velocity reduces the computed outflow through the southern channel, whereas the contribution of the northern channel brings the total outflow close to that computed using a single station (5% smaller). If the same correction is applied to observations, the total outflow would reduce to  $Q_2 = -0.78$  Sv. The paper also assesses the importance of eddy fluxes to the total outflow, their contribution being negligible ( $\leq 5\%$ ).

**Citation:** Sánchez-Román, A., G. Sannino, J. García-Lafuente, A. Carillo, and F. Criado-Aldeanueva (2009), Transport estimates at the western section of the Strait of Gibraltar: A combined experimental and numerical modeling study, *J. Geophys. Res.*, 114, C06002, doi:10.1029/2008JC005023.

### 1. Introduction

[2] The Strait of Gibraltar, with a length of around 60 km and 14 km width by its narrowest part, connects the Mediterranean basin with the Atlantic ocean. The seafloor raises from 2000 m depth in the Alboran sea, the Mediterranean side of the Strait, to about 800–900 m in its eastern entrance, the section between Gibraltar and Ceuta (Figure 1). West of this section the Strait, with depths still exceeding 800 m, narrows toward the minimum width section next to Tarifa, the so-called Tarifa Narrows. To the west, the bottom abruptly raises to the section of minimum depth off Point Camarinal, determining the so-called Camarinal Sill (CS hereinafter) section (maximum depth of  $\approx 290$  m, see CS in Figure 1). More to the west, the presence of a submarine ridge called Majuan Bank (MB) divides the outflowing cross-section into two channels. The northern channel has

a maximum depth of 250 m while the southern channel reaches depths of 360 m and forms the so-called Espartel Sill (ES hereinafter) that represents the main gateway of the Mediterranean outflow.

[3] The excess of evaporation ( $E$ ) over precipitation ( $P$ ) and river runoff ( $R$ ), together with the conservation of mass and salt in the Mediterranean basin drive the two-layer baroclinic exchange in the Strait of Gibraltar. This exchange has been traditionally described as an inverse estuarine circulation [*Stommel and Farmer, 1953*] with an upper flow  $Q_1$  of about 1 Sv ( $1 \text{ Sv} = 10^6 \text{ m}^3 \text{ s}^{-1}$ ) of fresh ( $S_A \approx 36.2$ ) and warm Atlantic Water spreading into the Mediterranean basin, and a lower flow  $Q_2$  of relatively cold and salty ( $S_M \approx 38.4$ ) Mediterranean Water that sinks into the Gulf of Cadiz down to a depth of about 1000 m, where it becomes neutrally buoyant [*Baringer and Price, 1997; Ambar et al., 2002*] before spreading into the North Atlantic. A long term barotropic flow  $Q_n = Q_1 - Q_2$  of the order of 0.05 Sv is necessary to balance the water deficit ( $E-P-R$ ) of the Mediterranean sea.

[4] The exchange is highly variable with strong fluctuations at semidiurnal frequency, less important but nonnegligible subinertial fluctuations in the range of few days to few

<sup>1</sup>Grupo de Oceanografía Física, University of Malaga, Malaga, Spain.

<sup>2</sup>Ocean Modelling Unit, ACS Division, C.R. Casaccia, Ente per le Nuove Tecnologie, l'Energia e l'Ambiente, Rome, Italy.

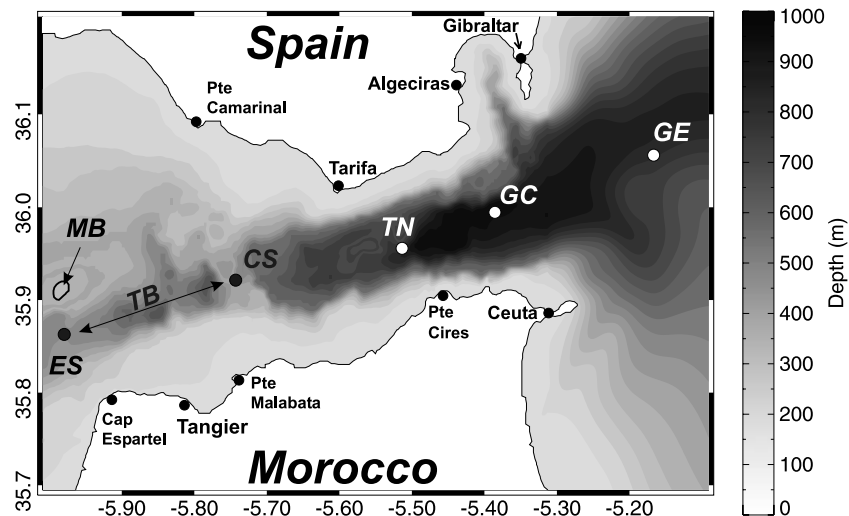


**Figure 1.** Map of the Strait of Gibraltar showing the location of the stations. The topographic features shown are Espartel Sill (ES), Tangier Basin (TB), Camarinal Sill (CS), Tarifa Narrows (TN). MB indicates the submarine ridge of Majuan Bank, which divides the Espartel section into two channels: the main channel to the south and a secondary one to the north.

weeks linked to meteorological forcing [Candela *et al.*, 1989; García-Lafuente *et al.*, 2002], and also seasonal and interannual variations. The analysis of this flow variability needs of long time series of velocity data. On the other side, the presence of strong tidal flows complicates the estimation of transports because semidiurnal tidal currents are strong enough to reverse the inflow and/or outflow in many places of the Strait during part of each tidal cycle [Candela *et al.*, 1990; Bryden *et al.*, 1994; García-Lafuente *et al.*, 2000], masking the two-layer character of the mean flow and making useless the concept of interface of null along strait velocity. Other definition of interface must be used to compute the transports at tidal frequencies. The usual choice is a surface of a given salinity, as initially suggested by Bryden *et al.* [1994]. They used  $S = 37.0$  at CS, while García-Lafuente *et al.* [2000] considered  $S = 37.8$  at the eastern section, after noticing that this salinity surface maximized the computed mean transports. Baschek *et al.* [2001], following the same approach but using a more comprehensive data set, found  $S = 38.1$  to be more adequate in this section. The different values used to define a salinity interface in different sections has to be ascribed to the entrainment and mixing that takes place along the strait. For this reason Sannino *et al.* [2004], using data from a numerical model, adopted as material interface the fortnightly averaged salinity surface, associated with the fortnightly averaged surface of zero along-strait velocity. The question of the interface at tidal frequencies is of concern in studies of water exchange due to eddy fluxes (positive correlations of tidal currents and tidally induced vertical displacements of the interface). They produce tidal rectification of the flow and contribute to the mean exchange by as much as 45% in CS [Bryden *et al.*, 1994; Tsimplis and Bryden, 2000; Vargas *et al.*, 2006] due to the large tidal excursions of the interface. Eddy fluxes are much less important in the eastern part of the Strait [García-Lafuente *et al.*, 2000; Baschek *et al.*, 2001] because tidal currents in

the upper layer are not strong enough to reverse the mean inflow.

[5] Computation of eddy fluxes has to be carried out at tidal frequencies, which in turn requires a material interface well defined throughout the tidal cycle. The alternative of using a surface of a given salinity is obviously restricted to cases where salinity profiles are available. If not, a second possibility is to use Acoustic Doppler Current Profiler (ADCP) data to find the surface of maximum vertical shear of the horizontal velocity, which would be identified with the interface [Tsimplis and Bryden, 2000]. It is a good assumption whenever the maximum shear coincides with the surface of null velocity, which is probably the case in CS, but not if the maximum shear is inside either layer. In these situations the surface of maximum shear is a proxy of the interface rather than the interface itself and a correction must be applied before accepting it as a realistic interface.

[6] The estimation of the exchanged flows from observations has technical and operational limitations. In practice, transports are computed using velocities recorded by few moorings (often only one) that do not resolve the cross-strait structure of the flow. Horizontal velocities at the sampling depths are assumed to be representative for the whole section at these depths. Moreover, the general lack of data in the first 40 or 50 meters of the water column makes the inflow be poorly determined from direct observations. The most recent and accurate estimates from direct measurements are probably the ones from Tsimplis and Bryden [2000], García-Lafuente *et al.* [2000] and Baschek *et al.* [2001]. These authors took into account the vertical displacements and the cross-strait variability of the velocity and determined the transport of the lower layer to be  $-0.67$  Sv over CS and  $-0.87$  Sv at the eastern section of the Strait respectively. In the last 15 years the exchange through the Strait of Gibraltar has also been studied by means of numerical models of different complexity, from one-dimensional models developed by Longo *et al.* [1992], Brandt *et al.* [1996] and Castro *et al.* [2004], to two-

dimensional models by *Tejedor et al.* [1999], *Izquierdo et al.* [2001], *Morozov et al.* [2002], to three-dimensional models by *Wang* [1989, 1993] and *Sannino et al.* [2002, 2004]. The only model able to provide realistic transports was that developed by *Sannino et al.* [2004]. Its high spatial resolution (less than 500 m in horizontal and 32 sigma levels) allows for a detailed description of the three-dimensional velocity and salinity pattern at semidiurnal tidal frequency and, therefore, the model accounts for eddy fluxes as well.

[7] Despite numerical models developed for the Strait of Gibraltar have reached in recent years a good level of accuracy, there is a lack of joint numerical and experimental approaches to study the exchange. This paper compares transport obtained from observations and computed using outputs from a high resolution numerical simulation. A recent three-yearlong series of good-quality observations is used to compute the part of Mediterranean outflow flowing through the southern channel of the ES, which is the main gateway for the outflow. The outputs of an improved version of the model developed by *Sannino et al.* [2004], are used to (1) evaluate the error introduced when only a vertical profile is used for the transport computation, (2) estimate the percentage of the outflow through the northern channel of ES where observations are not available, and (3) combine (1) and (2) to determine a correction for the outflow computed from observations through the southern channel in order to be representative of the whole outflow through ES.

[8] The paper is organized as follows: section 2 describes the observations, section 3 presents the model and its validation in the frequency band of tides which is by far the more complex to be simulated: should the model success within this band, it would be very reliable at other timescales. In section 4, the three years observations are processed to estimate the flow through the southern channel of ES and the observations during April months are compared with the output of the numerical model. The influence of the cross-strait structure of the flow and the relative importance of the northern channel are also explored. Section 5 summarizes our findings.

## 2. Data

### 2.1. Data Sets

[9] Velocity data collected in five points along the axis of the Strait during different experimental projects have been used in this study to validate the model in terms of velocity tidal components. The five positions are (Figure 1) Espartel and Camarinal Sills, Tarifa Narrows (TN), Gibraltar Center (GC), and Gibraltar East (GE).

[10] Data from ES are the most recent recorded in the Strait. The station was placed at  $35^{\circ} 51.7'N$ ,  $5^{\circ} 58.6'W$  in September 2004 in the southern channel and is part of the Spanish-funded INGRES project. It is equipped with an uplooking ADCP moored at 15 m above seafloor, and a point-wise current meter and an autonomous CT probe at 8 and 5 m above seafloor, respectively. The ADCP resolves 40 bins, 8-meter thick each, at a sampling rate of 30 min. Three years (September 2004–September 2007) of data between 50 and 328 m have been used in this work to estimate the outflow. A subset two-yearlong of the same data set (from September 2004 to September 2006) was

recently used by *García-Lafuente et al.* [2007] to analyze the composition of the outflow in terms of the main water masses of the western Mediterranean basin and by *Sánchez-Román et al.* [2008] to analyze the vertical structure of tidal currents over ES.

[11] CS station consisted of an ADCP placed near the bottom that provided current velocity between 54 m and 274 m every 60 min with 10 m bin size [see *Candela et al.*, 1990 for details]. A subset of this data set, from October 1995 to April 1996, has been used here. TN station consisted of a mooring line with six RCM 7-8 AANDERAA current meters, in April–May 2003. GC station provided data from October 1995 to May 1996 at six levels and, finally, EG also provided data at six depths from May to June 2003. A summary of the position, sampling depths and intervals and other details are presented in Table 1.

### 2.2. Data Processing

[12] ADCP data come from the westernmost moorings of ES and CS. Since instruments were placed few meters above the bottom, where horizontal and vertical movements due to drag are much reduced, the maximum acceptable ADCP inclination of  $20^{\circ}$  for reliable velocity measurements was never exceeded. No corrections on the depth of the bins were necessary.

[13] Mooring lines of standard current meters extend vertically much more than ADCP lines and are sensitive to flow drag. In some areas, velocity reaches values up to  $1.5 \text{ m s}^{-1}$  and instruments can be pushed down more than 200 m. For instance, the shallowest current meter of the GC line, moored at a nominal depth of 40 m to sample within the Atlantic layer (the “interface”  $S = 37.8$  is about 120 m on average), was eventually displaced to depths greater than 250 m. In such cases, measurements at a given nominal depth are contaminated with observations from deeper levels. In order to remove these spurious observations the following procedure has been developed:

[14] In a first step, the harmonic constants of the whole series collected by a given instrument are obtained. Then, the harmonic analysis is iteratively repeated after progressively removing observations taken far from the instrument’s nominal depth. To this aim the water column has been divided into 10 m thick cells. In a first iteration, measurements between the maximum depth registered ( $Z_{\text{max}}$ ) and  $Z_{\text{max}} - 10 \text{ m}$  are removed. The percentage of data remaining in this new series is computed and a new harmonic analysis is performed. Then, data between  $Z_{\text{max}} - 20$  and  $Z_{\text{max}}$  are removed and the same procedure is repeated. Successive removals go on until the data of the remaining series become insufficient to resolve successfully tidal constituents by harmonic analysis.

[15] Figure 2 illustrates the result of this algorithm for the uppermost current meter in GC using the major semiaxis of  $M_2$  constituent as control parameter. When the harmonic analysis is performed on the original series, the major semiaxis is  $23 \text{ cm s}^{-1}$  but it progressively decreases as the percentage of processed data (or, equivalently, the depth range) is reduced. The initial value is contaminated by data from the Mediterranean layer whenever the current meter was displaced vertically into this layer. As the iteration goes on and data from this layer are removed, the major semiaxis reduces and finally reaches a plateau when the percentage of

**Table 1.** Location and Characteristics of the Mooring Lines<sup>a</sup>

Mooring Line (Bottom Depth)	Instrument	Latitude (°N)	Longitude (°W)	Depth (m)	Length Series (days)	Sampling Rate (min)	Data Availability	Covered Period
ES (360)	ADCP	35°51.70′	05°58.60′		493.02	30	yes	09/04–09/07
CS (290)	ADCP	35°54.80′	05°44.70′		176.50	60	yes	10/95–04/96
TN (600)								04/03–27/03
TN1	CURM	35°57.58′	05°32.99′	30	23.37	2	no	
TN2	CURM	35°57.58′	05°32.99′	60	23.37	2	no	
TN3	CURM	35°57.58′	05°32.99′	90	23.37	2	yes	
TN4	CURM	35°57.58′	05°32.99′	140	23.37	2	yes	
TN5	CURM	35°57.58′	05°32.99′	190	23.37	2	yes	
TN6	CURM	35°57.58′	05°32.99′	290	23.37	2	yes	
GC (960)								10/95–05/96
GC1	CURM	35°59.97′	05°22.67′	40	176.50	60	yes	
GC2	CURM	35°59.97′	05°22.67′	70	176.50	60	yes	
GC3	CURM	35°59.97′	05°22.67′	140	176.50	60	yes	
GC4	CURM	35°59.97′	05°22.67′	200	176.50	60	yes	
GC5	CURM	35°59.97′	05°22.67′	360	176.50	60	yes	
GC6	CURM	35°59.97′	05°22.67′	800	176.50	60	yes	
GE (750)								05/03–06/03
GE1	CURM	36°03.35′	05°10.09′	30	11.98	2	yes	
GE2	CURM	36°03.35′	05°10.09′	60	32.99	2	yes	
GE3	CURM	36°03.35′	05°10.09′	90	32.99	2	yes	
GE3	CURM	36°03.35′	05°10.09′	140	32.99	2	yes	
GE5	CURM	36°03.35′	05°10.09′	190	32.99	2	yes	
GE6	CURM	36°03.35′	05°10.09′	340	32.99	2	yes	

<sup>a</sup>CURM stands for point-wise current meter. The ADCP in ES and CS sampled, respectively, 40 eight-meter bins and 22 ten-meter bins from 328-m depth (ES) and 274-m depth (CS), upward.

data analyzed is between 78% and 39%. This would indicate that the 78% of data were collected within an “homogeneous” layer with respect to  $M_2$  tidal velocity, which in turn suggests that the current meter was measuring velocity only in the Atlantic layer. Further reduction of the number of data analyzed makes the  $M_2$  semiaxis velocity decrease to zero due to the progressive lack of information. The depth range represented by this current meter is thus defined by the 78% uppermost available data, the percentage that stabilizes the major semiaxis. This value corresponds to 60 m depth so the effective depth range for this current meter is 40–60 m. The procedure has been repeated for each conventional current meter in TN and GC lines.

[16] On the other hand, and as a consequence of vertical displacements, during certain moments a given instrument registered velocity at depths that should have been sampled by another instrument that was in turn measuring at lower depths. Those data have replaced spurious values in the time series of the appropriate instrument. Except for the shallow-

est current meter of the line, all series have been refined by including observations from instruments situated above whenever they burst in the depth range of any other. Details of these depth ranges in the different lines, replacements carried out and results from the quality test are summarized in Table 2. In EG, these corrections do not apply because of the smallness of vertical displacements.

### 3. Numerical Model

#### 3.1. Model Description

[17] The numerical model used in this work is CEPOM, a modified version of the Princeton Ocean Model, the ocean circulation model developed in the late 1970s by *Blumberg and Mellor* [1987] to study both coastal and open ocean circulation.

[18] The first version of CEPOM was implemented by *Sannino et al.* [2002] with the introduction of the MPDATA algorithm, developed by *Smolarkiewicz* [1984], as advection scheme for tracers. This version was used to investigate

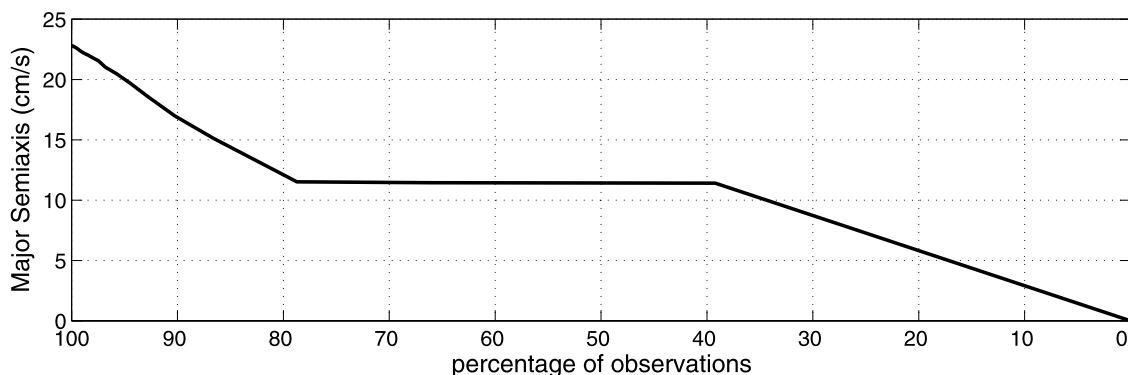


**Figure 2.** Quality test for GC1 time series. Y axis represents the value of  $M_2$  major semiaxis ( $\text{cm s}^{-1}$ ) obtained in the successive iterations of the process. X axis displays the percentage of data analyzed in each iteration. See text for details.

**Table 2.** Information of Data Processing<sup>a</sup>

Current Meter	Nominal Depth (m)	Vertical Range (m)	New Vertical Range (m)	Average Measure Depth (m)
TN3	90	111–161	111–150	122
TN4	140	145–220	161–200	172
TN5	190	212–314	213–280	228
TN6	290	309–370	318–360	322
GC1	40	40–277	40–60	51
GC2	70	63–300	63–80	71
GC3	140	117–338	117–135	126
GC4	200	168–370	168–180	174
GC5	360	284–397	284–299	291
GC6	800	775–882	775–803	789

<sup>a</sup>The nominal depth is the initially planned depth of instruments. Vertical range indicates the vertical displacement due to drag. New vertical range is the accepted depth interval represented by a given instrument, and the average depth is the assumed depth sampled by the instrument. It is the mean depth of all the retained observations (see text for details).

the mean exchange through the Strait of Gibraltar and was forced only by the density contrast between the Alboran Sea and the Gulf of Cadiz. CEPOM was further improved by *Sannino et al.* [2004] to study the semidiurnal tidal exchange through the Strait. Finally a version paralleled by means of the Scalable Modeling System tool (SMS) [*Govett et al.*, 2003] was used for describing the effect of the interfacial layer on transports and hydraulics in the Strait of Gibraltar [*Sannino et al.*, 2007].

[19] In this study, CEPOM has been improved using a higher resolution bathymetry and a new tidal forcing computed via OTIS package [*Egbert and Erofeeva*, 2002] that includes the main diurnal ( $O_1$ ,  $K_1$ ,  $P_1$ ) and semidiurnal ( $M_2$ ,  $S_2$ ,  $N_2$ ) tidal constituents. The initial conditions for salinity and temperature fields have been taken from the climatological Medar-MedAtlas Database [*MEDAR Group*, 2002].

[20] The model was initially run for 240 days without tidal forcing in order to achieve a steady exchange. Then the simulation extended for another 7 days forced by the 6 tidal constituents in order to achieve a stable time periodic solution. Finally the model was run for a further tropical month (27.321 days) that represents the main experiment. April climatological conditions were used in the simulation.

### 3.2. Model Validation

[21] In order to validate the numerical model, predicted and observed amplitude and phase of diurnal and semidiurnal tidal constituents of the along-strait velocity have been compared. Data for April months have been extracted from the different observed data set in ES, CS, TN, GC and GE and from the model simulation for the same locations and analyzed to obtain the harmonic constants [*Foreman*, 1978; *Pawlowicz and Lentz*, 2002]. One month series does not resolve the  $S_2$ - $K_2$  couple, which needs series of at least six months. For this reason,  $S_2$  harmonic constants are affected by its nonresolved companion unless inference is performed in the analysis [*Foreman*, 1978]. The amplitude ratio and phase difference between both constituents, which are necessary for inference, have been obtained from the analysis of longer time series in ES and CS.

[22] Figures 3–6 show the along-strait spatial distribution of amplitude and phase for each tidal constituent of observed and model data.

#### 3.2.1. Semidiurnal Constituents

[23] Spatial distribution of  $M_2$  amplitude is very similar for observed and model data (Figures 3a–3b). Local topog-

raphy forces a maximum amplitude of about  $120 \text{ cm s}^{-1}$  over CS. Values decrease toward the eastern and western ends of the Strait. The maximum value in the model is found shallower ( $\sim 60 \text{ m}$ ) than the observed one and there is a tendency for the model to give amplitudes slightly greater than observed. The agreement between observed and model  $M_2$  phase (Figures 3c–3d) is good, the differences being less than about  $15^\circ$  (time difference of 30 minutes) with earlier model phases west of CS and later phases to the east. An explanation could be the strong nonlinear frictional effects due to the abrupt topographic change west of CS, which are not properly solved in the model. Model and observed phases decrease toward the bottom, in accordance with the presence of a frictional boundary layer on a channel flow forced by a periodic pressure gradient [*Yasuda*, 1987].

[24] Figures 4a–4b show the spatial distribution of  $S_2$  amplitude, which reminds that of  $M_2$  with maximum value over CS ( $46 \text{ cm s}^{-1}$ ) and amplitude diminishing toward both ends of the Strait. The decrease is less stressed in the model, which gives place to higher model amplitudes. In TN a nearly depth-independent difference of about  $10 \text{ cm s}^{-1}$  is evident and in ES the model overestimates the peak velocity by about  $10 \text{ cm s}^{-1}$ . At the eastern end the agreement is better with differences less than  $5 \text{ cm s}^{-1}$  everywhere. The phase distribution of  $S_2$  (Figures 4c–4d) presents a pattern less organized than that of  $M_2$  with two cores of higher phases placed respectively west of CS, close to the bottom, and east of CS in the upper layer. A third relative maximum is detected at GE at about 350 m in the observed data while it is higher and shifted about 200 m upward in the model. As in  $M_2$  case the phase difference (obs-mod) is positive in and west of CS and negative east of it. Differences are less than  $20^\circ$ .

#### 3.2.2. Diurnal Constituents

[25] Spatial distribution of  $O_1$  amplitude is displayed in Figures 5a–5b. The model slightly underestimates the velocity, which is particularly evident over CS where the difference reaches its maximum value of  $10 \text{ cm s}^{-1}$ . Near the eastern and western limits of the Strait the difference diminishes, as the model predictions decrease more slowly toward the two ends of the Strait than the observed data. The  $O_1$  phase distribution (Figures 5c–5d) is more regular in the model than in the observed data. Highest phases locate near the surface and in the deep region east of CS and lower phases in the entire water column west of the sill. As a result, the maximum  $O_1$  velocity is reached before at

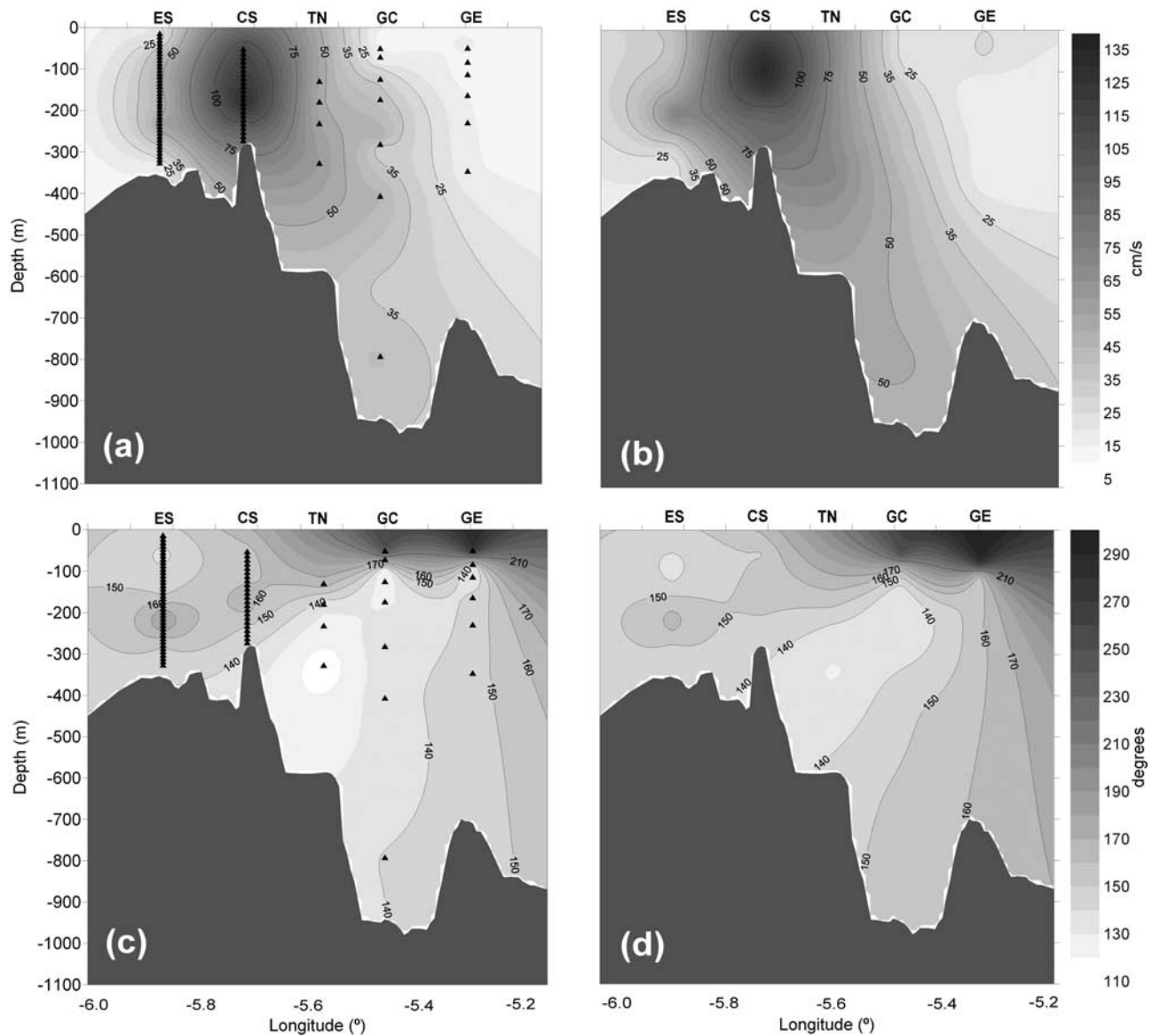


**Figure 3.** Tidal maps of the along-strait velocity:  $M_2$  constituent. (a) Observed amplitude. (c) Observed phase; solid triangles denote the points where observations are available. (b) Model amplitude using only the model outputs in the same locations as the observations. (d) Model phase. Amplitudes are  $\text{cm s}^{-1}$ ; phases are degrees referred to Greenwich transit.

middle depths east of CS and in the western part of the Strait. Observed phase has a more complex pattern and does not support the phase increase in the deep layer east of CS found in the model. The difference (obs-mod) is positive and reaches  $15^\circ$  (time difference of 60 minutes) west of CS and negative toward east ( $\sim 10^\circ$  at middle depths,  $\sim 20^\circ$  close to bottom).

[26] The spatial distribution of  $K_1$  amplitude is presented in Figures 6a–6b. The pattern is similar for observed and model data with, again, maximum values over CS that decay toward both ends of the Strait. As for  $O_1$ , the entire pattern reveals that the model underestimates the velocity reaching a maximum difference (obs-mod) of about  $10 \text{ cm s}^{-1}$  over CS. Close to the limits of the Strait, the difference decreases showing similar values at middepths at GC. Over GE, instead, model values are overestimated with a negative

difference (obs-mod) of about  $-4 \text{ cm s}^{-1}$ . Model and data phase distribution (Figures 6c–6d), are more alike than they were for  $O_1$ . A core of higher phases is found near the sea surface at GC and GE and lower phases are obtained close to the bottom. Phases differ by  $20^\circ$  and  $30^\circ$  at middle depths in GC due to the rapid decrease in the upper 150 m in observed data, which is not echoed by the model. West of CS, a zone of higher phases close to the bottom in the data is observed, which is less evident in model data, leading to a positive difference (obs-mod) of about  $20^\circ$  at the middle depths that rises to  $40^\circ$  close to the bottom over ES.

[27] Taking into account the great complexity and strong spatial variations of tidal currents in the Strait, the comparison of tidal charts for model and observations presented here can be considered quite satisfactory since differences are limited to less than  $10 \text{ cm s}^{-1}$  in amplitude and  $20^\circ$  in

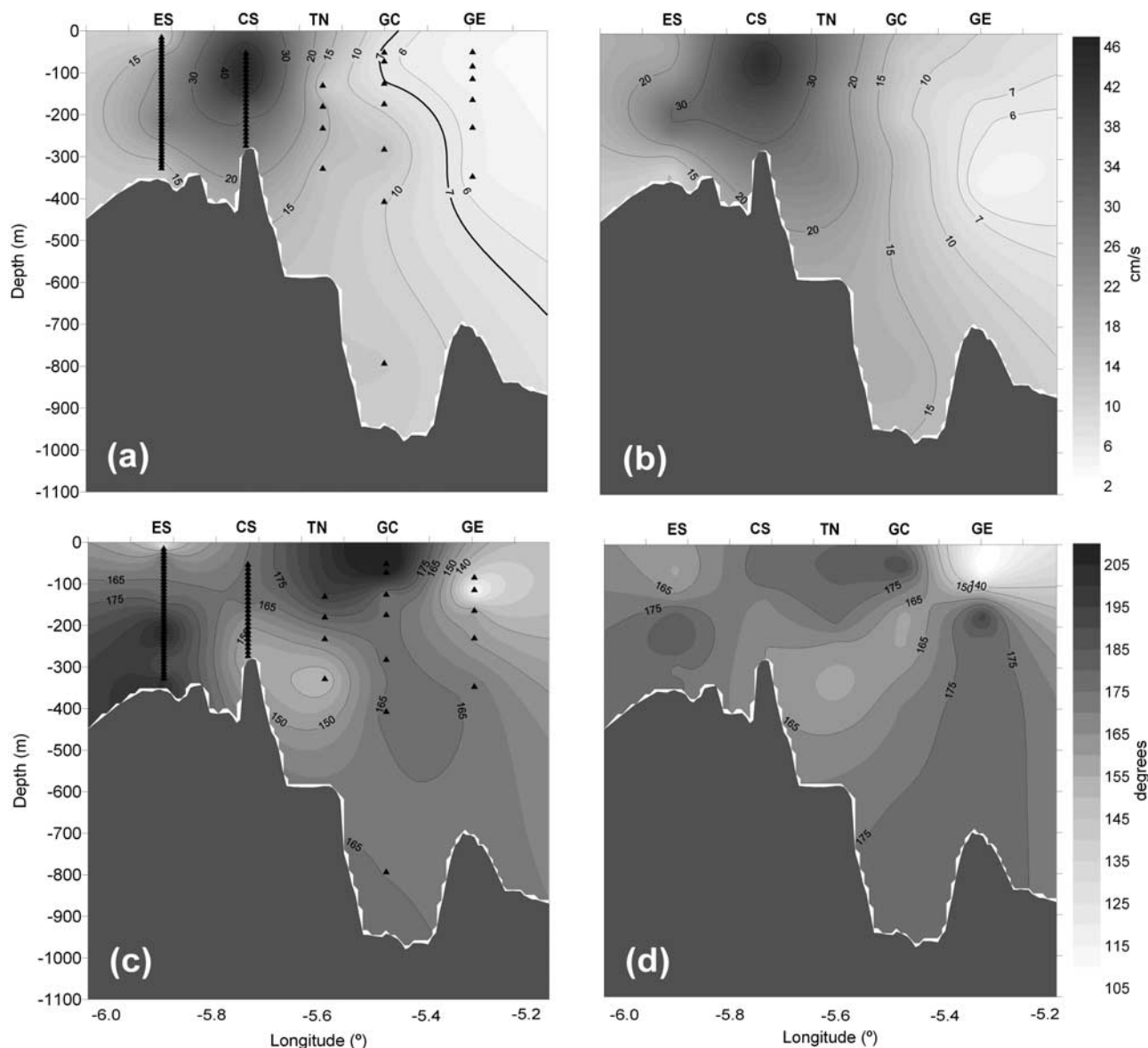


Figure 4. Same as in Figure 3, but for  $S_2$ .

phase in most part of the area. This reasonable good agreement builds confidence to use the model outputs to complement the observations when studying the dynamics of the exchange in other much less energetic, and therefore less conflictive, frequency bands.

#### 4. Mediterranean Water Transport at Espartel Sill

##### 4.1. Observations

[28] In this Section, the three-yearlong time series of ADCP data in ES is used to estimate the Mediterranean outflow through the southern channel of ES. As in other areas of the Strait, tidal currents also distort the two-layer exchange in ES during part of the tidal cycle, specifically during the flood (westward moving) tide, when all the water column moves toward the Atlantic. At first, the difficulty can be overcome by removing tidal fluctuations (a 8th order low-

pass Butterworth filter, FB1 hereinafter, with passband and stopband frequencies  $f_1 = 0.0263$  cph and  $f_2 = 0.0357$  cph has been used to this aim). The low-pass time series of observed currents show up a permanent two-way exchange and, hence, a well-defined interface of null velocity at a mean depth of about 190 m. Using the low-pass series the subinertial transport is computed according to

$$OUT(t) = \int_b^{h(t)} \langle u(z, t) \rangle W(z) dz, \quad (1)$$

where  $\langle u(z, t) \rangle$  is the along-strait low-pass velocity profile,  $W$  is the width of the southern channel at depth  $z$ , and  $h(t)$  is the time-dependent depth of the surface of zero low-pass velocity. This computation ignores the part of the outflow that flows north of Majuan Bank (see Figure 1) where observations are lacking. Transport through the secondary channel of Espartel will be addressed in section 4.2.2.

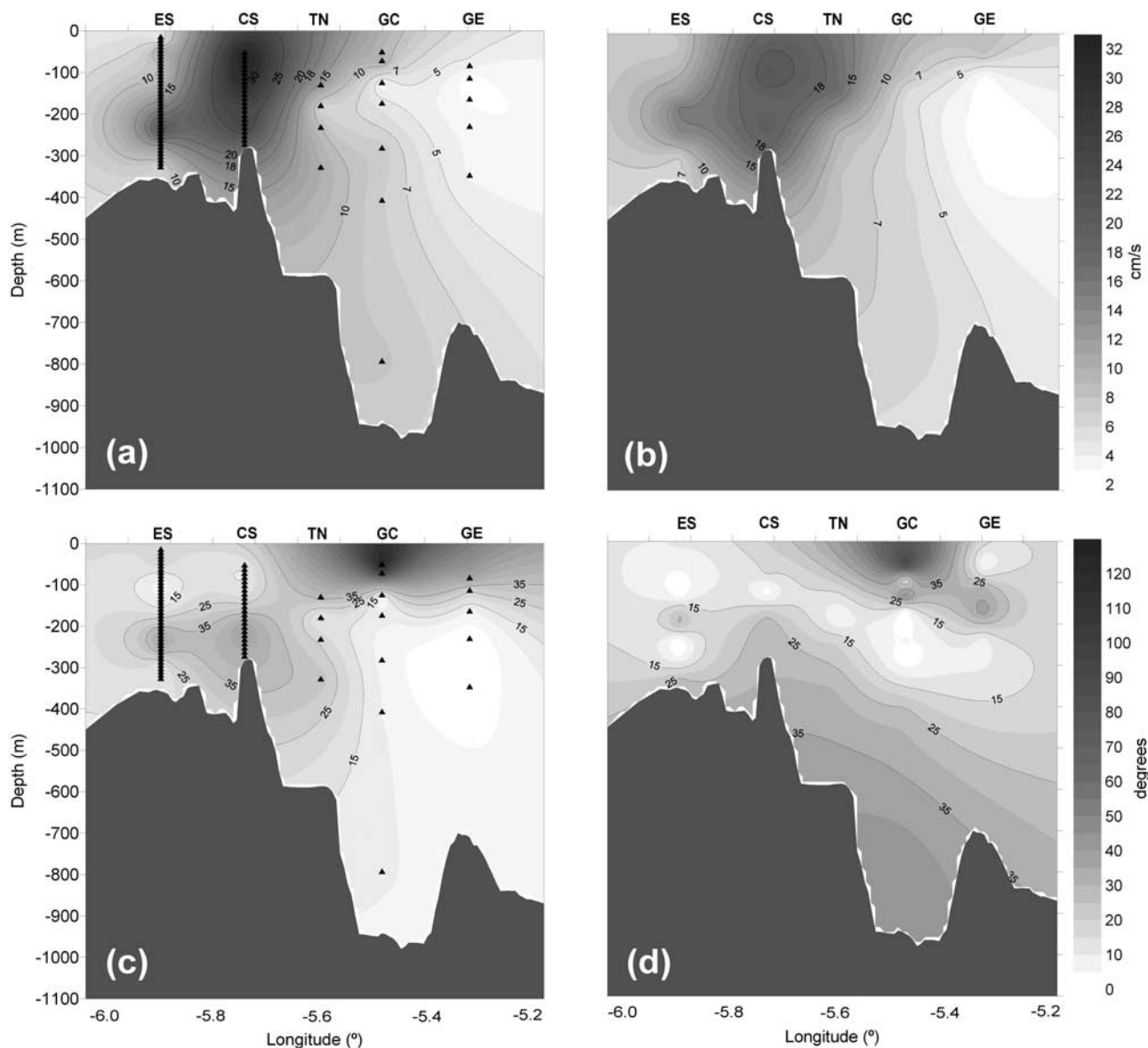


Figure 5. Same as in Figure 3, but for  $O_1$ .

[29] The resulting outflow (Figure 7a), has a mean value of  $Q_{2M} = -0.79 \pm 0.13$  Sv (subindex “M” hereinafter will refer to flows computed using low-pass series). The observed fluctuations are driven by atmospheric systems passing over the Mediterranean. Monthly means (Figure 7b) remove most of this variability and shows a clear seasonality with absolute maximum in April and minimum during autumn–early wintertime as well as marked interannual variability that makes April 2006 be the month of maximum transport ( $-0.93$  Sv).

[30] The previous computation is somewhat deceitful because it ignores eddy fluxes. As commented in Introduction, these eddy fluxes can be computed using ADCP data to estimate an “instantaneous” interface based on the position of the surface of maximum shear. In ES, the depth of maximum shear is 40 m below the surface of null low-pass velocity (Figure 8), inside the lower layer. For this reason, the “instantaneous” depth of maximum shear has been raised 40 m and used as the limit of integration in

equation (1). Model salinity profiles have been used to validate this correction: several isohalines were used to compute the exchanged flows in ES, and the maximum transport was obtained for  $S = 36.5$ , whose mean depth is 193 m, 3 meters below the surface of maximum shear after being corrected by the aforementioned distance of 40 m.

[31] The series of instantaneous transport,  $q_2(t)$ , has a mean value of  $-0.82 \pm 0.37$  Sv, with peaks exceeding  $-2.5$  Sv. The difference between  $Q_{2M}$  ( $-0.79 \pm 0.13$  Sv) and the new one would be the contribution of the eddy fluxes ( $-0.03$  Sv), which is around 4% of the computed outflow, a similar percentage to that found in the eastern part of the Strait [García-Lafuente et al., 2000; Baschek et al., 2001]. From  $q_2(t)$  we compute their subinertial variability by applying the FB1 filter to obtain  $Q_{2T}(t) = \langle q_2(t) \rangle$  (subindex “T” hereinafter will refer to flows computed by low-pass filtering the “instantaneous” flow).  $Q_{2T}(t)$  has the same timescale of variability as  $Q_{2M}(t)$  but they do not coincide.

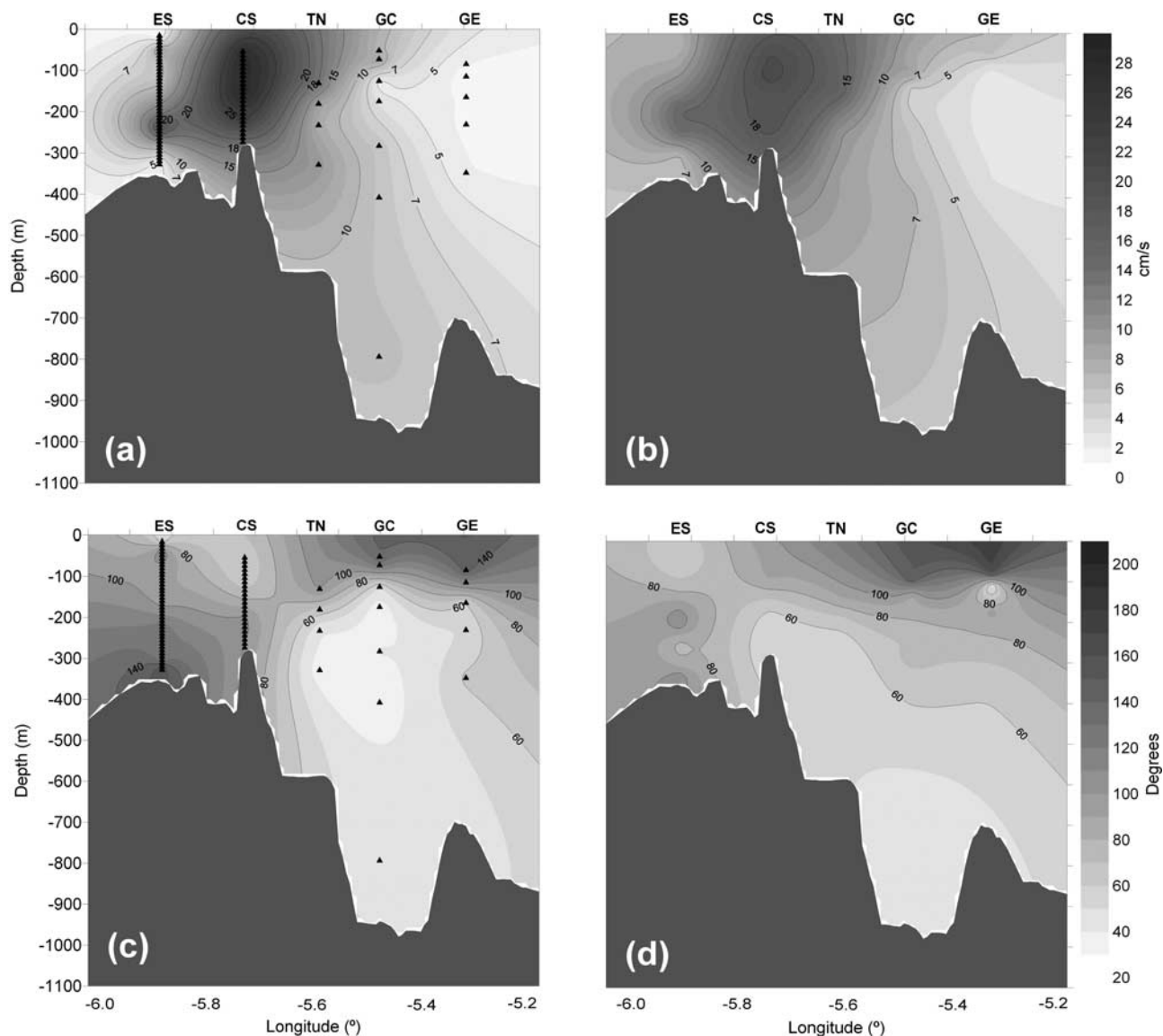


Figure 6. Same as in Figure 3, but for  $K_1$ .

The difference is identified as the contribution of eddy fluxes  $Q_{2E}(t)$  (subindex “E” will refer to eddy fluxes hereinafter).

[32] Figure 9 displays  $Q_{2T}(t)$ ,  $Q_{2M}(t)$  and  $Q_{2E}(t)$  between October 2006 and October 2007.  $Q_{2E}(t)$  is enhanced during spring tides due to higher vertical excursions of the interface, and it reduces to nearly zero during neap tides, a result also found by Vargas *et al.* [2006] in CS. Contrary to this case, the contribution of the eddy fluxes is negligible in the western part of the Strait, a fact that is surely related to the absence of full flow reversals in the lower layer, reversals that are the rule in CS almost every tidal cycle.

## 4.2. Model Results and Comparison With Experimental Data

### 4.2.1. Model Transport

[33] As model simulation was forced only by diurnal and semidiurnal tides and in order to compare model data with observations, the subinertial signal was removed from  $q_2(t)$  series by means of the empirical mode decomposition technique [Huang *et al.*, 1998]. The technique decomposes

the observed transport in contributions of different frequencies facilitating the removal of those associated to the meteorological forcing. Only diurnal and semidiurnal tidal contributions and the mean and long term trend were retained. The model was run for April climatological conditions so we use data of all available April (2005, 2006 and 2007) for comparison purposes. The observed total transport through the southern channel for this month is  $Q_{2TA} = -0.89$  Sv (subindex A indicates April), while  $Q_{2MA} = -0.85$  Sv and  $Q_{2EA} = -0.04$  Sv, 4% of the total outflow again. Notice that  $Q_{2TA}$  is greater (in absolute value) than  $Q_{2T}$  because of the seasonality of the flow (see Figure 7b). The ratio  $Q_{2EA}/Q_{2TA}$  is the same, however.

[34] Model velocity profile at ES from the simulated month was processed similarly as the observed data. The computed transport through the southern channel is  $Q_{2Tmod} = -1.03$  Sv, 0.14 Sv higher than  $Q_{2TA}$  in absolute value. The transport computed from the filtered series is  $Q_{2Mmod} = -0.96$  Sv, 0.07 Sv lower than  $Q_{2Tmod}$ , the difference attributed to eddy fluxes  $Q_{2Emod}$  that represents 7% of the total

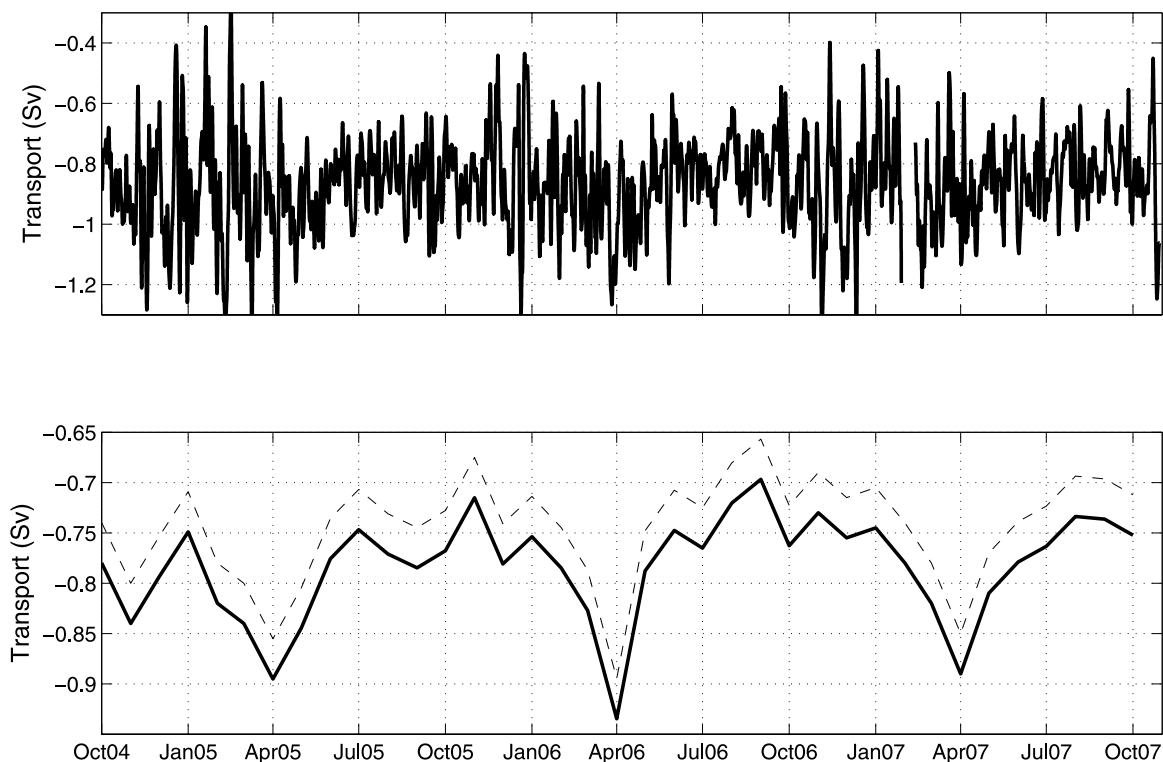


**Figure 7.** (a) Subinertial outflow through the southern channel of ES using the subinertial series of ADCP velocity. The series does not include eddy fluxes. (b) Monthly averages of the total outflow (including eddy fluxes) through the southern channel (solid line) and total outflow through ES (both north and south channels) deduced after correcting for cross-strait velocity structure and flow across the northern channel (dashed line).

outflow, a percentage greater than the 4% obtained with observed data.

[35] Comparison of model and observed (subindex “mod” and “A” respectively) transports shows that the former are about 15% greater than the observed because the model velocity at ES is slightly higher than observed velocity in the deepest levels (Figure 10). The interface is also somewhat shallower in the model (15 m above) and contributes to this difference as well.

#### 4.2.2. Effect of Cross-Strait Structure of Velocity on Transport Computation

[36] The previous transport computations have implicitly assumed that the single velocity profile at ES is representative

of the entire channel and have ignored the cross-channel structure of the flow. Model resolves this structure and allows for a more accurate computation of the outflow. Figures 11 and 12 display the velocities predicted in the entire ES section for spring and neap tides, respectively, and show that velocity is not uniform throughout the entire section but decreases toward the boundaries. The maximum outflow velocity is in the central part of the southern channel, south of Majuan Bank, which clearly implies a transport overestimation when using data from the center of the channel.

[37]  $Q_{2Tmod}$  transport has been recomputed integrating the along-strait velocity from the bottom to the depth of the interface defined by the surface of maximum shear, and then

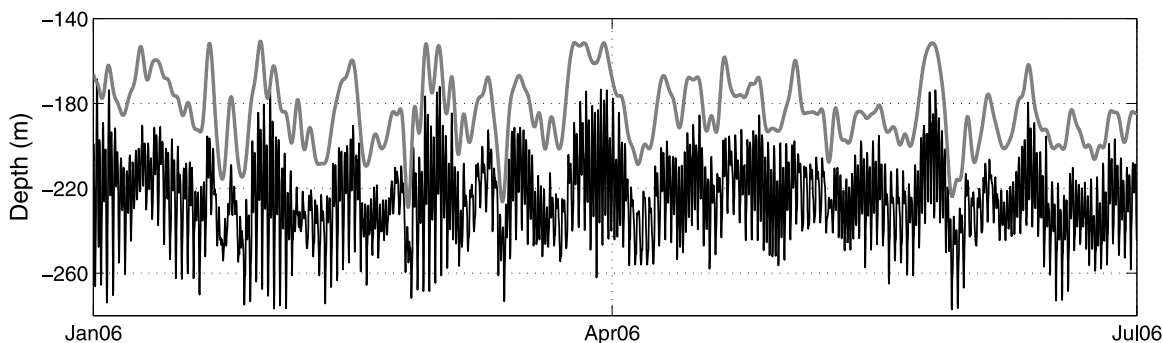


**Figure 8.** Interface between Atlantic and Mediterranean layers at ES. Black line is the “instantaneous” maximum shear surface, and gray line is the surface of null low-pass velocity surface. The mean difference is 40 m, the latter being shallower than the former.

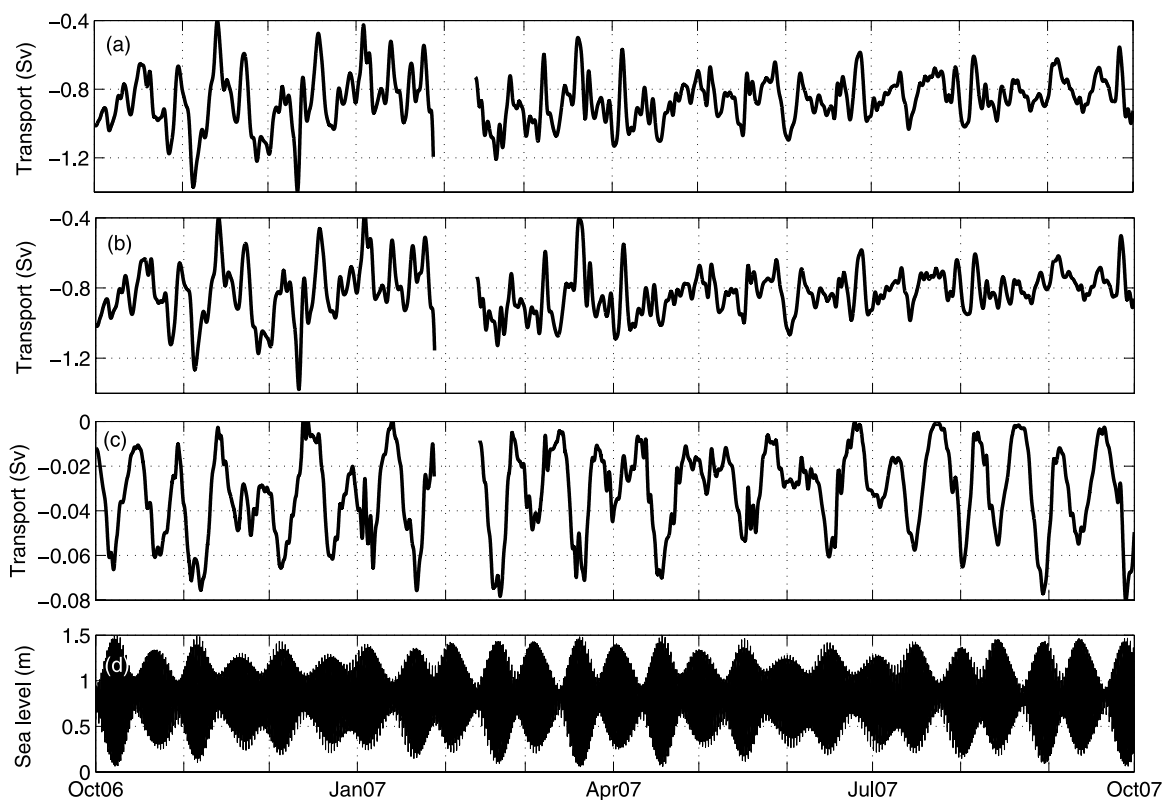


**Figure 9.** Outflow through the southern channel of ES from 1-year observations. (a)  $Q_{2T}$ . (b)  $Q_{2M}$ . (c)  $Q_{2E}$  (notice the change of Y scale). (d) Sea level at Tarifa. See text for the meaning of “T”, “M,” and “E” subindices.

meridionally across the ES section. The mean transport through the southern channel is  $Q_{2TmodSC} = -0.80$  Sv (subindex SC indicates south channel), 0.23 Sv lower than

that obtained from a sole velocity profile in the central part of the channel ( $Q_{2Tmod} = -1.03$  Sv, see Table 3). This result quantifies the flow overestimation in 22%.

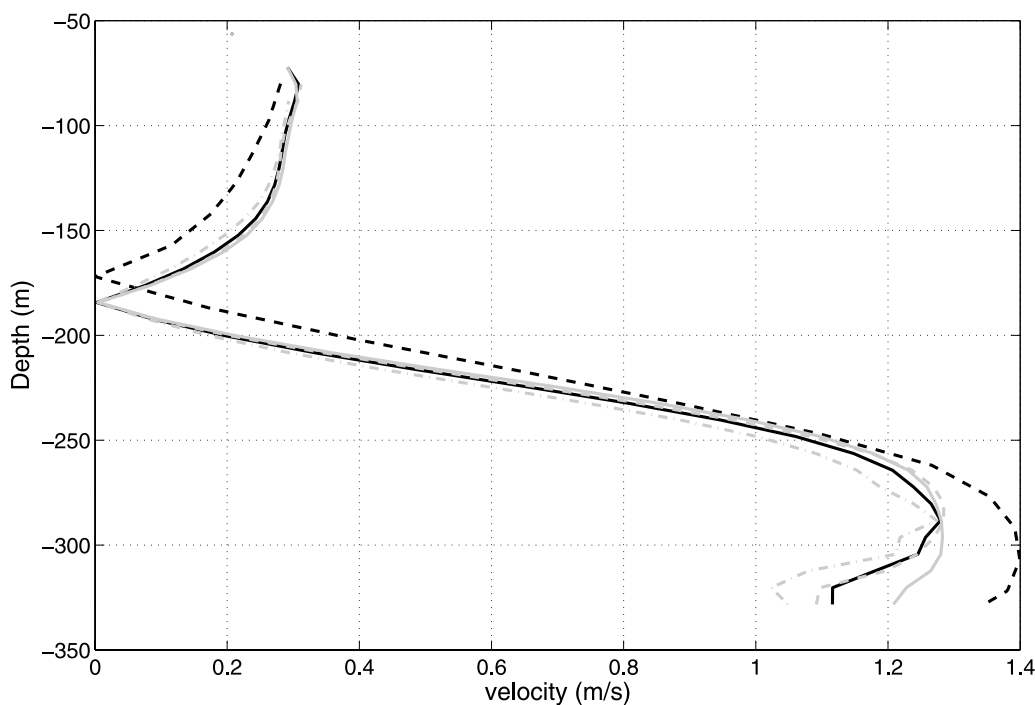


**Figure 10.** Mean profile of model (black dashed line) and observed (black solid line) velocities in ES. Gray lines are the mean velocity profiles of all available April (2005, 2006, and 2007).

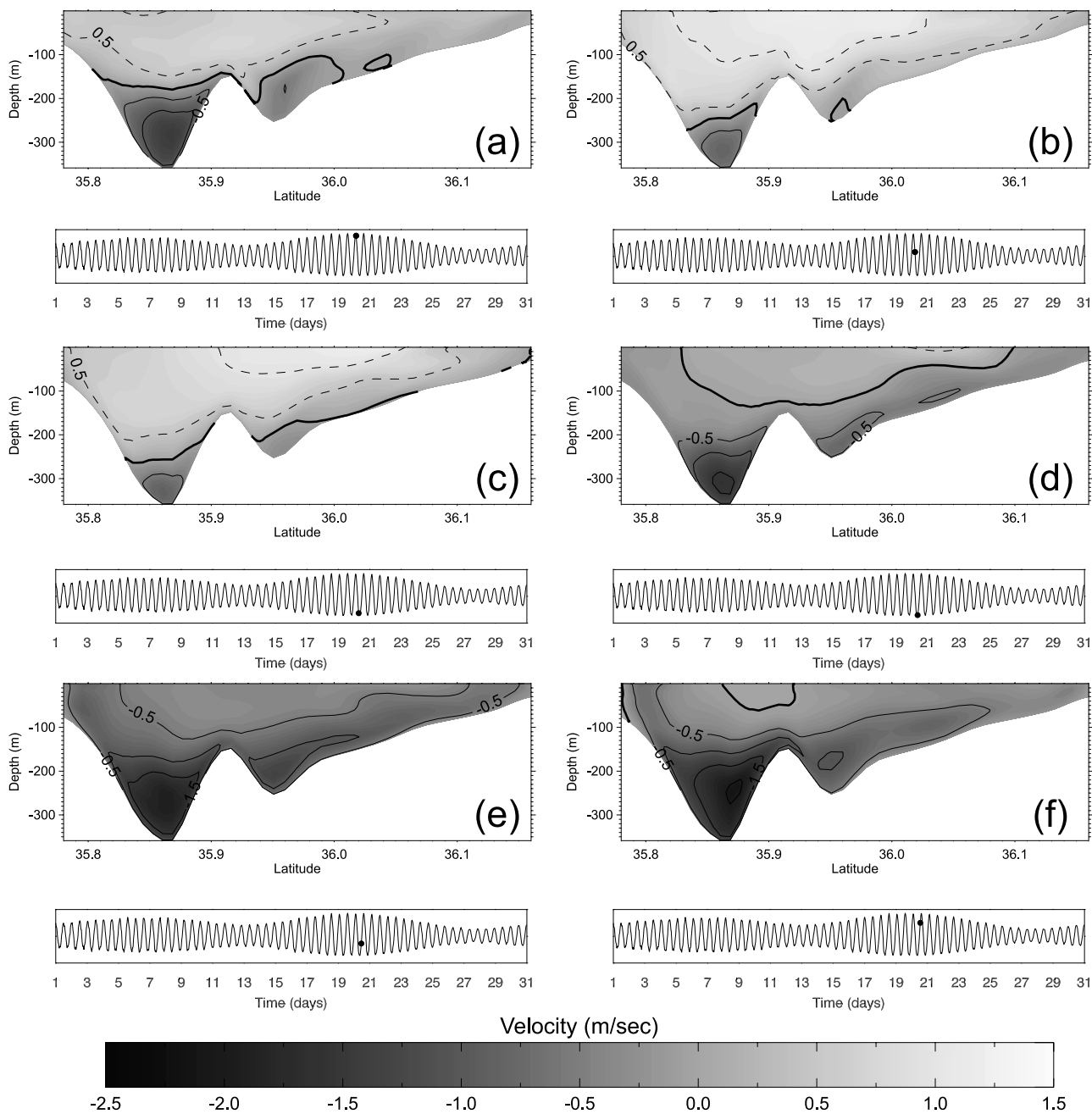


**Figure 11.** (a–f) Along-strait velocity across ES ( $\text{m s}^{-1}$ ) simulated by the model during spring tide. Solid lines indicate negative velocities (toward the Atlantic), and dashed lines indicate positive velocities (toward the Mediterranean). The thick line indicates zero velocity. Different snapshots are 2 hours apart. The tidal time, referred to the surface tide in Tarifa, is indicated at the bottom of each panel.

[38] Model data were also used to compute the fraction of Mediterranean water flowing through the secondary north channel of ES. They give a mean value of  $Q_{2TmodNC} = -0.18 \text{ Sv}$  (subindex NC indicates north channel). The total outflow adds up to  $-0.98 \text{ Sv}$ , 18% of which flows through the northern channel.

## 5. Summary and Conclusions

[39] A three-yearlong velocity time series collected in ES within INGRES projects together with velocity data collected in other four sites along the Strait axis during

different experimental projects have been used to validate a new improved version of the CEPOM numerical model in terms of the harmonic constants of the main tidal constituents. Taking into account the great complexity of tidal dynamics in the Strait, the comparison of tidal charts of the most important diurnal ( $O_1$ ,  $K_1$ ) and semidiurnal ( $M_2$ ,  $S_2$ ) constituents obtained from observations and data (Figures 3–6) is quite satisfactory with differences limited in most part of the strait to less than  $10 \text{ cm s}^{-1}$  in amplitude and  $20^\circ$  in phase. This good agreement supports the use of model results to correct the flow estimated from observations for those other dynamic features which are not resolved by the

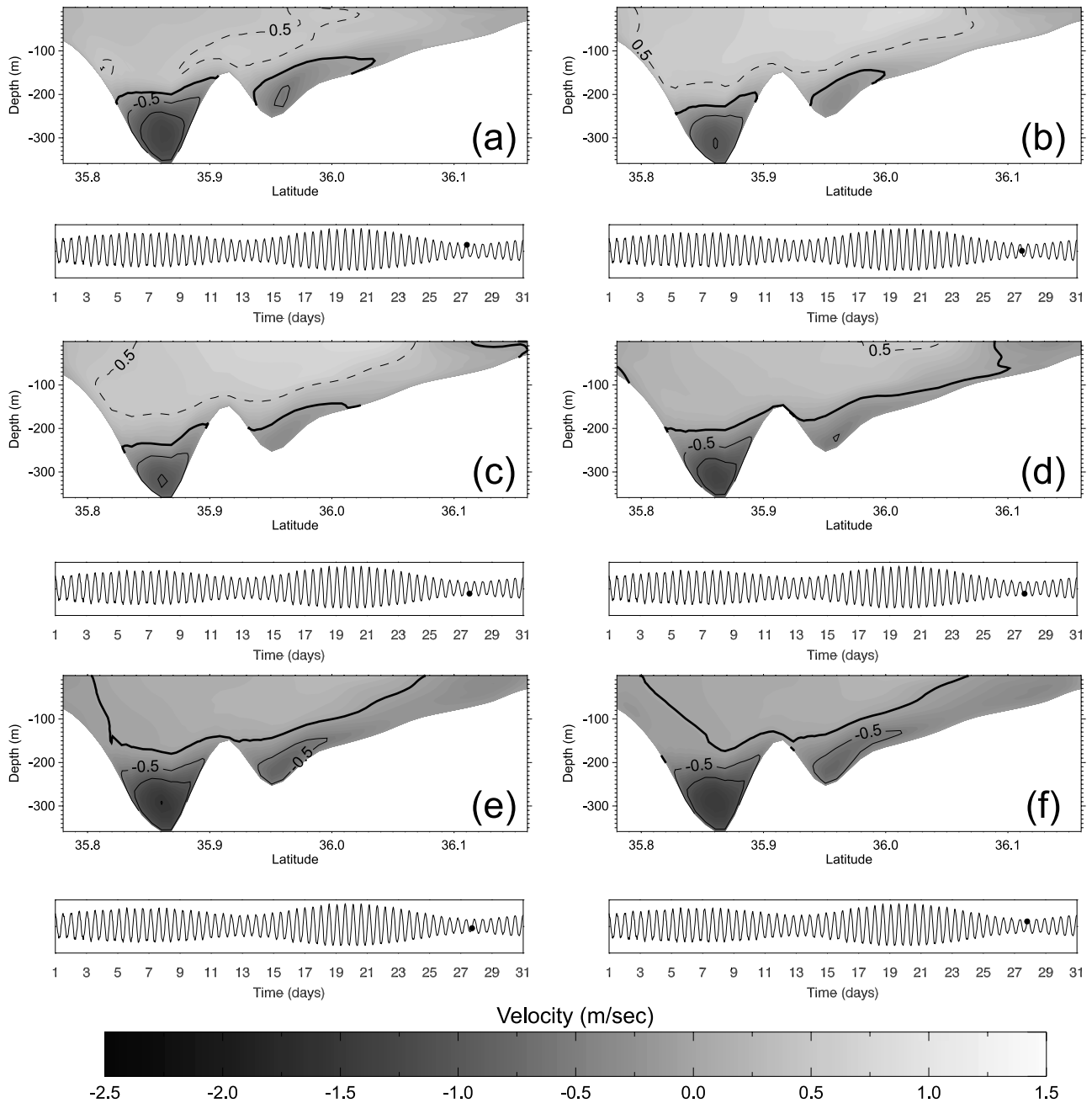


Figure 12. Same as in Figure 11, but for neap tide.

Table 3. Summary of the Different Values of Outflow (Sv) Mentioned in the Text<sup>a</sup>

	OBSERVATIONS		MODEL (Climatological April)			
	(Single Station, South Channel)		Single Station	Cross-Strait Structure		
	3-year Data	April Months	South Channel	South Channel	North Channel	Total
$Q_{2T}$	-0.82	-0.89	-1.03	-0.80	-0.18	-0.98
$Q_{2M}$	-0.79	-0.85	-0.96	-0.73	-0.17	-0.90
$Q_{2E}$	-0.03	-0.04	-0.07	-0.07	-0.01	-0.08

<sup>a</sup>In all cases, subindex “T” refers to the outflow computed from instantaneous values, subindex “M” is the outflow obtained using tidal-free time series of velocity and depth of the interface, and subindex “E” indicates eddy fluxes contribution to the outflow (see text for details). The rule “T” = “M” + “E” stands always. First column gives the outflow through the southern channel computed from 3-year observations at a single station; second column is the same for an “average” April month; third column presents the outflow computed from the model using exactly the same procedure as in column 2. Columns 4 and 5 give the values obtained from the model through the southern and northern channels, including the cross-strait structure of the flow. Last column is the total outflow through the full ES section from model data.

monitoring station at ES, such as the flow through the northern channel or the cross-strait structure of the flow.

[40] The flow through the southern channel computed from observations has been estimated in  $Q_{2T} = -0.82$  Sv ignoring the cross-structure of the flow but taking into account the contribution of eddy fluxes, which on the other hand have negligible influence (less than 4%), on total flow, as little bit enhanced during spring tides. The surface of maximum shear has proven to be a suitable proxy for computing the “instantaneous” outflow at tidal timescales, which is a previous necessary step for computing eddy fluxes. The series obtained exhibits seasonality with absolute maximum in April and minimum during autumn—early wintertime and marked interannual variability that makes April 2006 be the month of maximum transport.

[41] Since the model has been run for climatological conditions of April, data of all available April (2005, 2006 and 2007) have been averaged for comparison purposes. The model outflow has been computed with the velocity profile at the same site and using the same methodology as for observations and the comparison indicates that model transports are about 15% greater than the observed ones (Table 3). The reason is a somewhat higher model velocity at ES in the deep layers and also a shallower ( $\approx 15$  m) interface in the model.

[42] The model output is particularly suitable to provide corrections to the flow computed using a single profile of horizontal velocities. As mentioned above, a unique monitoring station cannot provide information about the cross-strait structure of the flow, neither about the importance of the outflow passing through the northern channel of ES. The model can fill these gaps and, therefore, it provides worthy information to assess the accuracy of the outflow estimations from observations at a single station. When the cross-strait structure of the velocity field is taken into account, the model indicates that the flow computed from a single station must be reduced around 22% due to lateral friction. The model also predicts an outflow through the northern channel of ES that represents around 18% of the total outflow (see Table 3 for details). Curiously, the final value the model predicts for the outflow considering the spatial structure and the northern channel contribution is nearly the same as that obtained from a single station through the southern channel ( $-0.98$  Sv versus  $-1.03$  Sv, compare third and last column in Table 3) because the reduction by friction through the southern channel is about the same as the net flow through the northern one. If this difference of around 5% is maintained in the observations, then the value of  $-0.82$  Sv deduced from the three-yearlong series would be reduced to  $-0.78$  Sv, a result that agrees well with the  $-0.76 \pm 0.07$  Sv reported by *Baschek et al.* [2001] from ADCP observations with an inverse tidal model over the eastern part of the Strait. This procedure can be used to obtain the transport through the whole ES section when only the observations at the single station in the southern channel are available.

[43] **Acknowledgments.** The data analyzed in this work were collected within the frame of the Spanish-funded projects INGRES (REN03-01608/MAR) and INGRES-2 (CTM06-02326/MAR). We thank the Spanish Ministry of Science and Technology for financial support. ASR acknowledges a postgraduate fellowship from this Ministry. CS data have been kindly provided by Dr. Julio Candela, CICESE, Ensenada, Mexico. We also thank the crews of *R/V Odon de Buen* and *R/V Francisco de Paula*

*Navarro* from Instituto Español de Oceanografía for help, assistance, and a well-done work during the deployment and recovering of the mooring lines in the often unfriendly environment of the Strait of Gibraltar. This work was initiated when ASR was visiting the ACS Division, Ocean Modeling Unit, ENEA, C.R. Casaccia in Rome. The ES monitoring station is part of the Mediterranean Sea monitoring network Hydro-Changes, sponsored by the CIESM. Partial support has been received from P07-RNM-02938 Spanish-funded project.

## References

- Ambar, I., N. Serra, M. J. Brogueira, G. Cabecadas, F. Abrantes, P. Freitas, C. Goncalves, and N. Gonzalez (2002), Physical, chemical and sedimentological aspects of the Mediterranean Outflow off Iberia, *Deep-Sea Res. Part II*, *49*(19), 4163–4177.
- Baringer, M. O., and J. F. Price (1997), Mixing and spreading of the Mediterranean Outflow, *J. Phys. Oceanogr.*, *27*(8), 1654–1677.
- Baschek, B., U. Send, J. García-Lafuente, and J. Candela (2001), Transport estimates in the Strait of Gibraltar with a tidal inverse model, *J. Geophys. Res.*, *106*(C12), 31,033–31,044.
- Blumberg, A. F., and G. L. Mellor (1987), A description of a three-dimensional coastal circulation model, in *Coastal and Estuarine Sciences 4: Three Dimensional Coastal Models*, edited by N. S. Heaps, pp. 1–16, AGU, Washington, D.C.
- Brandt, P., W. Alpers, and J. O. Backhaus (1996), Study of the generation and propagation of internal waves in the Strait of Gibraltar using a numerical model and synthetic aperture radar images of the European ERS1 satellite, *J. Geophys. Res.*, *101*(C6), 14,237–14,252.
- Bryden, H., J. Candela, and T. Kinder (1994), Exchange through the Strait of Gibraltar, *Prog. Oceanogr.*, *33*(3), 201–248.
- Candela, J., C. Winant, and H. L. Bryden (1989), Meteorologically forced subinertial flows through the Strait of Gibraltar, *J. Geophys. Res.*, *94*, 12,667–12,674.
- Candela, J., C. Winant, and A. Ruiz (1990), Tides in the Strait of Gibraltar, *J. Geophys. Res.*, *95*(C5), 7313–7335.
- Castro, M., J. García-Rodríguez, J. González-Vida, J. Macías, C. Pares, and M. Vázquez-Cendon (2004), Numerical simulation of two-layer shallow water flows through channels with irregular geometry, *J. Comput. Phys.*, *195*, 202–235.
- Egbert, G. D., and L. Erofeeva (2002), Efficient inverse modeling of barotropic ocean tides, *J. Atmos. Ocean. Technol.*, *19*, 183–204.
- Foreman, M. G. G. (1978), *Manual for Tidal Currents Analysis and Prediction*, *Pacific Marine Sci. Rep.* 78-6, 57 pp., Inst. of Ocean Sci., Patricia Bay, Sydney, B. C.
- García-Lafuente, J., J. Vargas, F. Plaza, T. Sarhan, J. Candela, and B. Baschek (2000), Tide at the eastern section of the Strait of Gibraltar, *J. Geophys. Res.*, *105*(C6), 14,197–14,213.
- García-Lafuente, J., E. Alvarez-Fanjul, J. Vargas, and A. Ratsimandresy (2002), Subinertial variability through the Strait of Gibraltar, *J. Geophys. Res.*, *107*(C10), 3168, doi:10.1029/2001JC001104.
- García-Lafuente, J., A. S. Roman, G. D. del Rio, G. Sannino, and J. S. Garrido (2007), Recent observations of seasonal variability of the Mediterranean outflow in the Strait of Gibraltar, *J. Geophys. Res.*, *112*, C10005, doi:10.1029/2006JC003992.
- Govett, M., L. Hart, T. Henderson, J. Middlecoff, and D. Schaffer (2003), The scalable modeling system: Directive-based code parallelization for distributed and shared memory computers, *Parallel Comput.*, *129*, 995–1020.
- Huang, N. E., Z. Shen, S. Long, M. Wu, H. Shih, Q. Z. N. Yen, C. Tung, and H. Liu (1998), The empirical mode decomposition and Hilbert spectrum for nonlinear and non-stationary time series analysis, *Proc. R. Soc. London A*, *454*, 903–995.
- Izquierdo, A., L. Tejedor, D. V. Sein, J. O. Backhaus, P. Brandt, A. Rubino, and B. A. Kagan (2001), Control variability and internal bore evolution in the Strait of Gibraltar: A 2-d two-layer model study, *Estuarine Coastal Shelf Sci.*, *53*, 637–651.
- Longo, A., M. Manzo, and S. Pierini (1992), A model for the generation of nonlinear internal tides in the Strait of Gibraltar, *Oceanol. Acta*, *15*, 233–243.
- MEDAR Group (2002), Medatlas/2002 database. Mediterranean and Black Sea database of temperature salinity and bio-chemical parameters. Climatological atlas, European Commission Marine Science and Technology Programme (MAST), *IFREMER ed.*
- Morozov, E. G., K. Trulsen, M. Velarde, and V. Vlasenko (2002), Internal tides in the Strait of Gibraltar, *J. Phys. Oceanogr.*, *32*, 3193–3206.
- Pawlowicz, B. B. R., and S. Lentz (2002), Classical tidal harmonic analysis including error estimates in matlab using t-tide, *Comput. Geosci.*, *28*, 929–937.
- Sánchez-Román, A., F. Criado-Aldeanueva, J. García-Lafuente, and J. S. Garrido (2008), Vertical structure of tidal currents over Espartel and

- Camarinal sills, Strait of Gibraltar, *J. Mar. Sys.*, *74*, 120–133, doi:10.1016/j.jmarsys.2007.11.007.
- Sannino, G., A. Bargagli, and V. Artale (2002), Numerical modeling of the mean exchange through the Strait of Gibraltar, *J. Geophys. Res.*, *107*(8), 3094, doi:10.1029/2001JC000929.
- Sannino, G., A. Bargagli, and V. Artale (2004), Numerical modeling of the semidiurnal tidal exchange through the Strait of Gibraltar, *J. Geophys. Res.*, *109*, C05011, doi:10.1029/2003JC002057.
- Sannino, G., A. Carillo, and V. Artale (2007), Three-layer view of transports and hydraulics in the Strait of Gibraltar: A three-dimensional model study, *J. Geophys. Res.*, *112*, C03010, doi:10.1029/2006JC003717.
- Smolarkiewicz, P. (1984), A fully multidimensional positive definite advection transport algorithm with small implicit diffusion, *J. Comput. Phys.*, *54*, 325–362.
- Stommel, H., and H. Farmer (1953), Control of salinity in an estuary by a transition, *J. Mar. Res.*, *12*, 13–20.
- Tejedor, L., A. Izquierdo, B. Kagan, and D. Sein (1999), Simulation of the semidiurnal tides in the Strait of Gibraltar, *J. Geophys. Res.*, *104*(C6), 13,541–13,557.
- Tsimplis, M., and H. Bryden (2000), Estimation of the transports through the Strait of Gibraltar, *Deep Sea Res. Part I*, *47*(12), 2219–2242.
- Vargas, J., J. García-Lafuente, J. Candela, and A. Sanchez (2006), Fortnightly and monthly variability of the exchange through the Strait of Gibraltar, *Prog. Oceanogr.*, *70*(2–4), 466–485.
- Wang, D. (1989), Model of mean and tidal flows in the Strait of Gibraltar, *Deep-Sea Res.*, *36*, 1535–1548.
- Wang, D. (1993), The Strait of Gibraltar model: Internal tide, diurnal inequality and fortnightly modulation, *Deep Sea Res. Part I*, *40*(6), 1187–1203.
- Yasuda, H. (1987), Vertical structure of the tidal current ellipse in a rotating basin, *J. Oceanogr. Soc. Jpn.*, *43*, 309–318.

---

A. Carillo and G. Sannino, Ocean Modelling Unit, Special Project Global Climate ENEA C.R. Casaccia, Ente per le Nuove Tecnologie, l'Energia e l'Ambiente, SP 91 Via Anguillarese 301, S.M. Galeria, I-00060 Rome, Italy.  
F. Criado-Aldeanueva, J. García-Lafuente, and A. Sánchez-Román, Grupo de Oceanografía Física, E.T.S.I. Telecomunicación, Universidad de Málaga, Campus Teatinos s/n, C.P. E-29071 Malaga, Spain. (antonio.sanchez@ctima.uma.es)